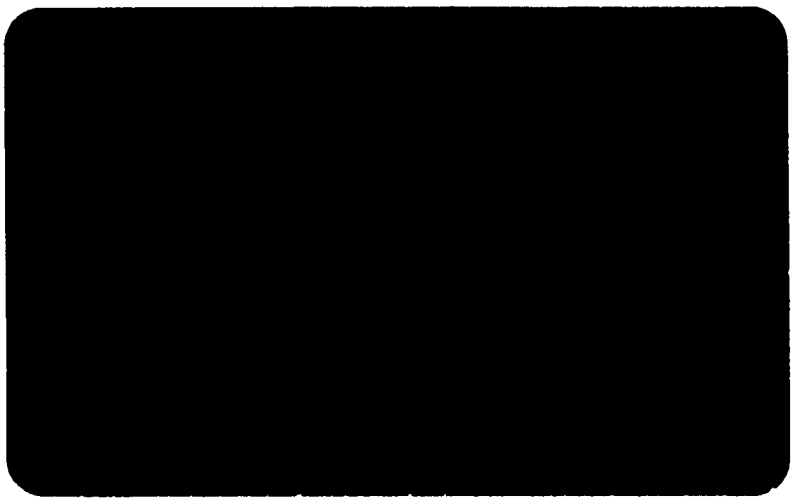

J Delft
niversity of Technology

Faculty of Aerospace Engineering

THRUST-VECTORED WINDSHEAR RECOVERY

Memorandum M-845

H.G. Visser

This memorandum has been prepared in the framework of a joint NLR/TUD project

TU Delft
Delft University of Technology

June 1998

DELFT AEROSPACE
FACULTY OF AEROSPACE ENGINEERING

Title : Thrust-vectored Windshear Recovery

Author(s) : H.G. Visser

Abstract : This study presents a preliminary evaluation of the application of Thrust Vector Flight Control (TVFC) technology for improving windshear recovery of civil aircraft in a microburst encounter on final approach. A numerical trajectory optimization technique based on the method of multiple shooting is applied to achieve a microburst escape with minimal loss of altitude for a Boeing 727 type aircraft. Although the application of TVFC does result in a slight improvement in recovery altitude, there is also a price to paid in the sense that TVFC utilization significantly hampers the ability to gain specific energy during recovery. Maintaining an energy buffer during a microburst encounter is highly desirable to achieve robustness with respect to uncertainties in windshear size and strength. TVFC aided windshear recovery has been compared with an alternative approach to improve the windshear survivability capability, namely the application of lateral maneuvering. This comparison learns that lateral maneuvering is not only a far more effective means to improve the recovery altitude, it also vastly improves energy preservation. One of the advantages of TVFC is that it permits operation at very high angles-of-attack. Although in the present point-mass analysis the issue of an increase in the permissible angle-of-attack range has not been exhaustively addressed, initial findings indicate that the energy management problems only become more pronounced. In conclusion, the findings regarding the use of TVFC for windshear recovery are insufficient to warrant a continuation of the research effort.

Keyword(s) : Thrust vectoring, optimal control problems, microburst escape strategies, windshear recovery, energy management.

Issue	1		
Date	June 1998		
Prepared	H.G. Visser		
Verified			
Approved			

Table of Contents

Nomenclature

AOA	-	Angle-of-attack
C_D, C_L	-	Aerodynamic coefficients
D	-	Drag force
E	-	Specific energy
g	-	Acceleration of gravity
h	-	Altitude
F	-	F-factor
J	-	Performance index
L	-	Lift force
r	-	Radial distance to microburst center
S	-	Wing area
T	-	Thrust
t	-	Time
V	-	Airspeed (TAS)
W	-	Aircraft gross weight
W_h	-	Vertical windspeed
W_r	-	Radial (horizontal) windspeed
W_x, W_y	-	Horizonal windspeed components
x, y, z	-	Position coordinates of aircraft
x_c, y_c	-	Horizontal position coordinates of microburst center
α	-	Angle-of-attack
β	-	Throttle response
β_t	-	Throttle setting
γ	-	Flight path angle
δ	-	Thrust inclination/Thrust vector angle
μ	-	Aerodynamic roll angle
ρ	-	Air density
τ	-	Time constant
χ	-	Heading angle
χ_w	-	Horizontal wind direction

Subscripts

0	- initial value
max	- maximum value
min	- minimum value
ref	- reference value

Superscript

*	- optimal value

1. Introduction

Recently the technology of Thrust Vectoring (TV), originally conceived for application to military aircraft, has been proposed to improve the safety of commercial jet aircraft[1,2,3]. TV technology enables the propulsive force of an aircraft engine to be directed to a desired angle relative to the vehicle body. Typically, the jet stream is deflected by paddles or special nozzles. Adapting military TV to present-day civil aircraft is certainly feasible, but depends on the specific combination of aircraft configuration, engine type and nozzle type. The feasibility of incorporating TV technology into an existing jet transport was demonstrated in the proof-of-concept study reported in Ref.2, involving a scale model of the Boeing 727-100. The aim of this particular study was to apply TV to civil jet transport aircraft in the form of simple add-on kits that do not impose any change on the engines but transform the vehicle into a much safer passenger aircraft.

Unlike for military aircraft, TV is not very effective for the augmentation of direct lift. The reason for this is simply the fact that the installed thrust levels in civil aircraft are usually substantially lower than the levels encountered in military aviation. However, in both civil and military aviation TV can be very useful to replace or augment conventional AFC (Aerodynamic Flight Control) elements, especially in the high angle-of-attack/low-speed flight regime. Indeed, TVFC (Thrust Vectoring Flight Control) is nearly independent of the airflow, which makes it significantly more effective in low speed situations than conventional aerodynamic control.

The aircraft configuration plays an important role in the provision of TVFC. Configurations featuring rear-mounted engines, such as the Boeing 727, provide the largest feasible pitch-moment arm and are therefore probably the most promising candidates in terms of potential TVFC safety benefits. Indeed, for thrust vectoring flight control of rear-mounted engine configurations relatively small thrust angle deflections, e.g., 20°, are sufficient to obtain the envisioned benefits. The potential safety benefits include, stall prevention and stall recovery (improved stability and controllability at low speeds), TVFC regaining control after engine failure and TVFC replacing one or more aerodynamic flight control elements that have failed (e.g. due to loss of hydraulics or elevator blockage).

The capability of TV to deal with loss of control is likely to be an important asset when encountering hazardous weather phenomena such as windshear. It is well known that windshear may seriously degrade aircraft performance, especially during low-level low-speed operations (take-off or landing). Windshear refers to spatial wind gradients that result from variations in wind speed or direction relative to an earth-fixed reference frame. Such wind changes engender an inertia force that influences an aircraft's energy state and, consequently, its flight path. A flight safety hazard arises when during the take-off or landing phase a sustained energy-draining windshear takes away energy at a faster rate than the engine thrust can add back. When entering such a condition, the airplane is forced to either lose airspeed, altitude or both, regardless of the control actions taken by the pilot.

Probably the most dangerous windshear phenomenon is the so-called microburst. A microburst is a strong downdraft that occurs when a column of air at high altitude quickly cools due to evaporation of ice, snow or rain. This cooling air becomes denser than the surrounding atmosphere and, as a result, rapidly descends to he ground. Upon nearing the ground, the downward moving air spreads out horizontally in all directions. The radially divergent winds subsequently evolve in one or more circular vortices, encircling the downflow (see Figure 1).

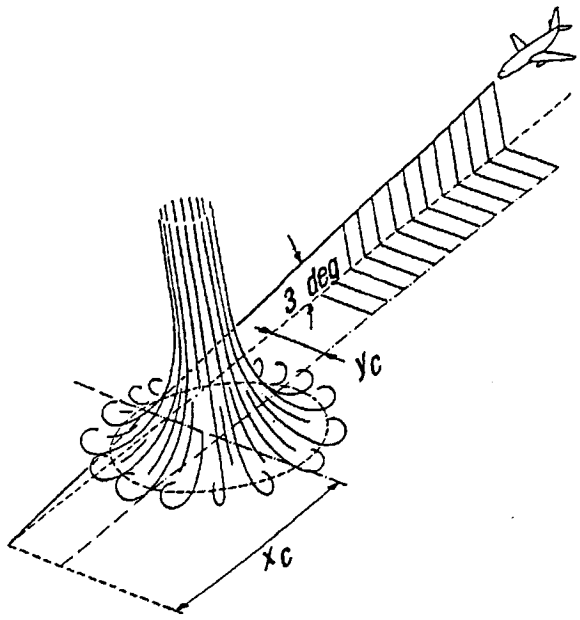

Figure 1. Microburst encounter during final approach.

The hazard of a microburst arises principally from its deceptive nature. An airplane which penetrates the center of a microburst in straight flight will initially experience an increasing headwind, which will actually enhance performance. However, as the aircraft proceeds the downdraft increases and the headwind shifts into a tailwind, causing the aircraft to lose energy.

Optimum energy management in windshear conditions depends on two key factors, viz., a timely recognition and an appropriate response. What flight crew response is appropriate in a windshear situation critically depends on how much advance warning is provided by the available windshear detection sensor(s) and what feedback information is available to the crew to enable the response.

In the event of late detection, avoidance of a microburst may not be feasible, and piloting strategies are then required that offer the best possible survival capability. Since we seek to avert an impending crash, a natural choice for the objective of an optimum recovery strategy is the maximization of the terrain clearance, or in other words, the maximization of the minimum altitude at any point along the escape trajectory (a problem of the so-called minimax or Chebyshev type). Typically, optimal performance is obtained by gradually exchanging airspeed for altitude with the minimum airspeed occurring at the very end of the shear.

When a microburst is inadvertently encountered a pilot of an aircraft is generally unsure where and when the high-shear region will end, particularly when the aircraft is equipped with an in situ sensor only. To make an aircraft less vulnerable to uncertainties in microburst size, strength and location, a pilot may attempt to limit the energy drain due to windshear, such as to reduce the risk of reaching the stall angle-of-attack while the aircraft

still is in the high-shear region. Unfortunately, however, any attempt to minimize the airplane total energy loss typically comes at the expense of a lower recovery altitude and therefore a compromise between the two conflicting requirements must be made. In a severe microburst a good compromise boils down to controlling the flight path such as not to hit the ground with excess airspeed or to stall at excess altitude.

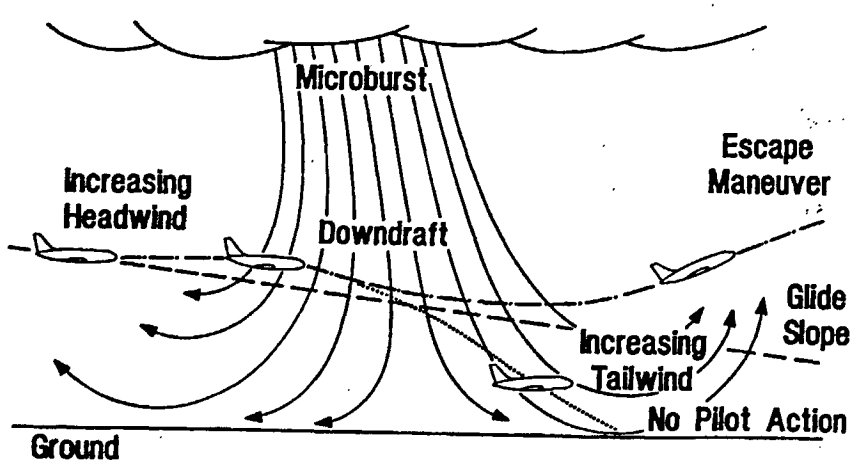

Figure 2. Microburst escape maneuver.

One of the most significant products that has emerged in the continuous struggle against the windshear threat is the so-called FAA Windshear Training Aid (WTA), which came out in 1987[4]. The significance of the WTA is not just related to the fact that it superseded the inadequate windshear flight training procedures that existed at the time, but above all, it heightened the overall awareness with respect to windshear hazards. Before the inception of the WTA, a common technique for escape in which many pilots throughout the world were trained, was to fly at the stick-shaker angle-of-attack. The idea was that this particular technique would offer certain performance advantages. The introduction of the WTA led to the recognition that deliberate attempts to fly at the stick-shaker angle-of-attack may actually seriously degrade the possibility for escape from a severe windshear. The recovery strategy proposed in the WTA is designed to be used in the absence of any flight director guidance. Indeed, the pilot is instructed to set maximum rated thrust and to rotate the airplane toward an initial pitch attitude of 16°. If this pitch attitude does not result in level or climbing flight, then pitch attitude should be further increased in small increments, while respecting the stick-shaker. The required pitch attitude then needs to be maintained until a positive rate of climb is established. The WTA also stipulates that an airplane should not be reconfigured (flap and gear retraction) during an escape maneuver.

In addition to its quaint simplicity, the WTA strategy has several attractive features,

including robustness with respect to uncertainties in windshear intensity and extent, and near-optimal performance. Although the WTA strategy generally performs satisfactory, significant research efforts have been devoted to the development of even better recovery strategies. These improvements in recovery performance are brought about by attempting to emulate the characteristics of the trajectories established in dynamic trajectory optimization studies[5,6,7,8]. Optimal control studies to improve the take-off and penetration landing performance during microburst encounter[9,10] have been performed, along with studies that specifically deal with the abort landing. The latter issue forms the starting point for the present study, in which we seek to establish the potential performance and safety benefits of thrust vectoring in a windshear encounter. As a matter of fact, the present work basically extends on previous work[7,8] on windshear recovery by adding a pitch thrust vectoring capability to a conventional jet transport aircraft model featuring rear-mounted engines (Boeing 727).

It has to be noted that the work presented herein is fairly restricted in scope in the sense that the dynamic optimization studies have been limited to point-mass vehicle models only. In other words, the rotational dynamics will be completely disregarded This implies that one of the main benefits of TVFC, namely overcoming loss of controllability in the high angle-of-attack/low-speed regime will not be considered. The unique TVFC capability of permitting post-stall maneuvering will also be ignored. Indeed, TVFC can be very useful in assisting pitch-AFC in recovering from a stall situation. Of main importance in this respect is quick recovery, such as to minimize the resulting altitude drop. In the present study, we actually seek to avoid stall by respecting the stick-shaker angle-of-attack limit at all times. However, in order to obtain an indication of the influence of TVFC at low airspeeds, we will also consider some scenario's that feature a slight increase in the stick-shaker angle-of-attack limit.

The main focus of the present study is to assess the impact of thrust vectoring on the aircraft survival capability under windshear conditions. As mentioned before, two aspects are important is this respect, viz. recovery altitude and energy management. More specifically, the objective is to investigate how much improvement in recovery altitude can be obtained through thrust vectoring, without sacrificing the build-up of an "energy reserve" in the after-shear phase of the microburst encounter.

The organization of this report is as follows. Details concerning the dynamic system model are described in Chapter 2. Next, the mathematical optimization problem is formally stated. In Chapter 4 the characteristics of open-loop optimal solutions are investigated for various scenario's. In the concluding Chapter the prospects for the proposed TVFC concept for civil applications is discussed.

2. Dynamic System Modeling

Using a relative wind-axes reference-frame[6], the equations of motion, describing the thrust-vetcored aircraft dynamics (represented by a point-mass model) in the three-dimensional space can be written as:

$$\dot{x} = V\cos\gamma\cos\psi + W_x \tag{1}$$

$$\dot{y} = V\cos\gamma\sin\psi + W_y \tag{2}$$

$$\dot{h} = V\sin\gamma + W_h \tag{3}$$

$$\dot{E} = \frac{[\beta T_{max}(1 - \frac{(\alpha+\delta)^2}{2}) - D]V}{W} + \dot{W}_h - \frac{V}{g}[\dot{W}_x\cos\gamma\cos\psi + \dot{W}_y\cos\gamma\sin\psi + \dot{W}_h\sin\gamma] \tag{4}$$

$$\dot{\gamma} = \frac{g}{V}[\frac{L + \beta T_{max}(\alpha+\delta)}{W}\cos\mu - \cos\gamma] + \frac{1}{V}[\dot{W}_x\sin\gamma\cos\psi + \dot{W}_y\sin\gamma\sin\psi - \dot{W}_h\cos\gamma] \tag{5}$$

$$\dot{\psi} = \frac{g}{V\cos\gamma}\frac{L + \beta T_{max}(\alpha+\delta)}{W}\sin\mu + \frac{1}{V\cos\gamma}[\dot{W}_x\sin\psi - \dot{W}_y\cos\psi] \tag{6}$$

$$\dot{\beta} = \frac{1}{\tau}[\beta_t - \beta] \tag{7}$$

where x, y and h are the position coordinates, E is the specific energy, γ is the flight path angle, ψ is the heading angle and β the throttle response. The wind velocity vector has three components, viz., W_x, W_y and W_h. The above set of equations is not essentially different from the set of equations used in previous studies[6,7,8]. As a matter of fact, the only difference is brought about in the interpretation of the variable δ. In contrast to previous studies, where δ represents a fixed inclination relative to the zero-lift axis, in the present TVFC study δ is used to define the effective pitch thrust-vectoring angle. It is assumed here that all three engines are rotated over the same angle. In addition, it is assumed that the magnitude of the thrust (T_{max}) is not affected by the TVFC. In view of

the relatively small deflection range that we will consider, the latter assumption is not likely to produce significant errors. A small angle approximation has been employed in the equations of motion for the thrust vector components along and perpendicular to the airspeed vector respectively, i.e., $\cos(\alpha+\delta) \approx 1 - \frac{1}{2}(\alpha+\delta)^2$ and $\sin(\alpha+\delta) \approx (\alpha+\delta)$. Although this assumption is not strictly necessary, it does simplify the optimal control analysis significantly. In addition, the following assumptions apply: (i) the wind flow field is steady, (ii) zero angle-of-sideslip, (iii) a flat non-rotating earth, and (iv) the aircraft weight is constant.

Due to the introduction of TVFC the number of controls is increased from three to four in the mathematical model :

(i) The throttle setting β_t constrained by:

$$0 \leq \beta_t \leq 1 \tag{8}$$

(ii) The aerodynamic roll angle μ which is limited by:

$$|\mu| \leq \mu_{max} \tag{9}$$

(iii) The angle-of-attack α which is forced to remain within the range:

$$0 \leq \alpha \leq \alpha_{max} \tag{10}$$

(iv) The thrust-vector angle δ which can be varied within the range:

$$\delta_{min} \leq \delta \leq \delta_{max} \tag{11}$$

The aerodynamic forces (lift L and drag D) are modeled as functions of airspeed V, altitude h and the angle-of-attack α :

$$L = C_L(\alpha)\, qS = \left[L_0 + L_1\alpha + L_2(\alpha - \alpha_{ref})^2\right]\tfrac{1}{2}\rho V^2 S \tag{12}$$

$$D = C_D(\alpha) qS = \left[D_0 + D_1\alpha + D_2\alpha^2\right]\tfrac{1}{2}\rho V^2 S \tag{13}$$

The maximum thrust is assumed to be a function of airspeed only, i.e.:

$$T = \beta T_{max}(V) = \beta\left(T_0 + T_1 V + T_2 V^2\right) \tag{14}$$

Generally speaking, the maximum thrust also depends on altitude, but this dependence has been ignored here in view of the fairly modest altitude variations in the microburst escape maneuvers.

As mentioned earlier, the aircraft type used in the investigation is a Boeing 727. Details of the original aerodynamic and thrust data for the unmodified aircraft type (in landing configuration) are summarized in Table 1.

Table 1 : aerodynamic and thrust data of the original B-727 aircraft model.

$W = 667233$ N , $S = 144.9$ m^2 , $\tau = 3$ sec , $\delta = 2°$		
T_0	$= 198280$ N	
T_1	$= -350.08$ N(m/s)$^{-1}$	
T_2	$= 0.69063$ N(m/s)$^{-2}$	
D_0	$= 0.15751$	
D_1	$= 0.0768$ rad^{-1}	
D_2	$= 2.524$ rad^{-2}	
L_0	$= 0.7076$	
L_1	$= 5.97$ rad^{-1}	
L_2	$= 0$	if $0 \leq \alpha \leq \alpha_{ref}$
	$= -5.95$ rad^{-2}	if $\alpha_{ref} \leq \alpha \leq \alpha_{max}$
α_{ref}	$= 0.2269$ rad	
α_{max}	$= 0.3002$ rad	

The introduction of TVFC is assumed not to affect any of the above data, excepting the thrust angle δ. Moreover, in some scenario's the stick-shaker angle limit will be increased from 17.2° to 18.2°. This 1° increment in stick-shaker angle-of-attack is fairly arbitrary.

Clearly, what we seek to do is to investigate the sensitivity of the optimal solution with respect to the stick-shaker limit. It needs to be mentioned that the manufacturer has supplied aerodynamic data for angle-of attack values up to 17.2° only. This implies that the aerodynamic data used in the present study has been essentially obtained through extrapolation. This obviously may have serious consequences with respect to the validity of the employed model. The consequences of the increased stick-shaker angle of attack in terms of stability/controllability have not been assessed at all.

Figure 3 shows that the relationship lift coefficient C_L versus angle-of-attack α, corresponding to the data listed in Table 1. The relationship shown is linear, up to 13° angle-of-attack. For larger values of the angle-of-attack, the established relationship is only slightly nonlinear. In view of the fact that the drag coefficient C_D is also represented by a quadratic polynomial in α, the increase in the stick-shaker limit does result in a drop in the value of the characteristic parameter C_L/C_D :

$$\frac{C_L}{C_D} = 6.048 \quad for\ \alpha = 17.2° \qquad (15)$$

$$= 5.852 \qquad = 18.2°$$

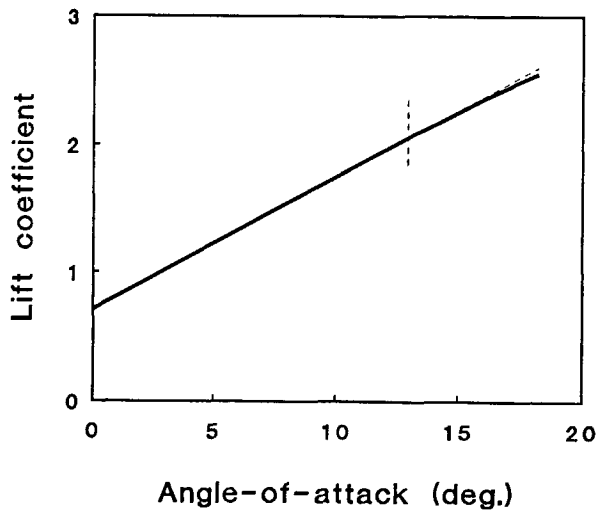

Figure 3. Lift coefficient versus angle-of-attack for Boeing 727.

For thrust vectoring flight control of the rear-mounted engine configuration of the Boeing 727 a relatively small thrust angle deflection range will be assumed:

$$-5° \leq \delta \leq 20° \qquad (16)$$

The microburst wind field flow model employed in this study concerns the well-known axisymmetric Soesman model, also used in previous studies[6,7,8]. For this reason a further description of the details is omitted here. It is recalled though, that polar coordinates have been used to describe the flow field in a horizontal plane (see Fig. 4). The employed analytic approximation of the flow field characteristics actually features separate models for the radial flow W_r (which may lead to horizontal shear) and the downdraft W_h. Note that the horizontal wind component W_r is only a function of the radial distance to the microburst center, whereas the vertical wind component W_h also depends on altitude to ensure that W_h decreases with decreasing altitude and has a stagnation point (i.e., zero vertical windspeed) at ground level.

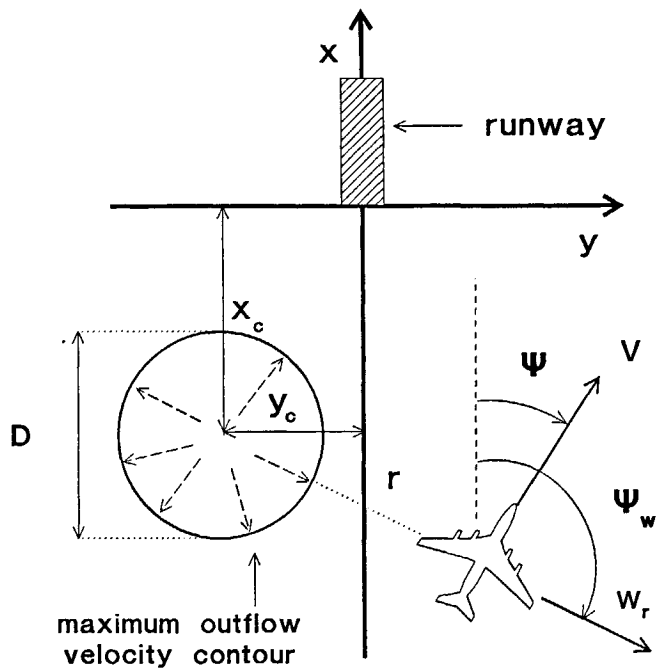

Figure 4 : Geometry of microburst encounter.

From Figure 4 it is readily clear that for a given aircraft position (x,y), the radial distance r from the microburst center (axis of symmetry) located at the point (x_c, y_c), can be computed from the relation:

$$r = \sqrt{(x - x_c)^2 + (y - y_c)^2} \tag{17}$$

Also observe that in the present study the origin of the coordinate frame is located at the runway threshold. Using polar coordinates, the horizontal wind components W_x and W_y can be readily related to the radial wind velocity W_r:

$$W_x = \cos\psi_w W_r(r) \quad ; \quad W_y = \sin\psi_w W_r(r) \quad , \tag{18}$$

where ψ_w is the direction of the radial wind velocity vector.

The wind terms in Eq.(4) that describe the windshear impact on aircraft specific energy parameter can be combined in a single characteristic parameter, called the F-factor:

$$F \triangleq \frac{(T-D)}{W} - \frac{\dot{E}}{V} \tag{19}$$

The F-factor can be interpreted as the loss or gain in available specific excess thrust due to the combined effect of downdraft and horizontal windshear. The F-factor therefore represents a direct measure of the degradation of an aircraft's potential climb gradient due to the windshear. Note that positive values of the F-factor indicate a performance decreasing situation.

Previous optimization studies have addressed the issue whether the most appropriate escape maneuver is a straight ahead climb or an evasive turning maneuver[6,7,8]. The idea here was that by turning the aircraft away from the microburst center, rather than flying straight through, the hazards caused by penetrating the microburst can potentially be reduced. The findings in these studies revealed that lateral maneuvering may indeed improve an aircraft's survivability, provided that the maneuver is not initiated too deep in the microburst core. In the current study, we will therefore also include scenario's that feature lateral maneuvering. However, only modest banking will be permitted. This is facilitated by prescribing fairly low values (up to 15°) for the aerodynamic roll angle limit in Eq.(9). For nonturning escape maneuvers, the roll angle limit has been set to zero.

It is important to emphasize that thrust vectoring is not only useful to improve the vertical turn rate, but also the horizontal turn rate will be affected when a lateral escape maneuver is executed. This becomes readily evident upon inspecting Eqs.(5) and (6). Indeed, the thrust vector remains in the aircraft's plane of symmetry, thus contributing to both the vertical and horizontal turn-rate components. On the other hand, Eq.(4) makes clear that for deflecting the thrust vector a price has to be paid in terms of a reduction in the available specific excess power. As has been mentioned before, the overall effect can a priori be expected to be limited, simply because of the fairly modest values of both the maximum deflection angle δ_{max} (20°) and thrust-to-weight ($T_{max}/W \approx 0.26$).

3. Optimal Control Formulation

3.1 Specification of the Performance Index for the Minimax Windshear Problem

In this Chapter the optimal control statement major established earlier in Refs.6 through 8 are reiterated, primarily for the purpose of identifying the implications of incorporating thrust vectoring in the system model formulation. First, we formally restate the performance index that we seek to optimize. As already pointed out in the introduction, the objective in this study is to minimize the peak value of the altitude drop (see Figure 5), which can be expressed by the Chebyshev (or minimax) functional :

$$I^* = \min I = \min \left[\max_t \left(h_{ref} - h(t) \right) \right] , \quad 0 \le t \le t_f , \tag{20}$$

where h_{ref} is a constant reference altitude and $[0,t_f]$ is the fixed flight time interval. Based on a well-known result obtained using functional analysis, i.e.,

$$\lim_{k \to \infty} \left[\int_0^{t_f} \left(h_{ref} - h(t) \right)^{2k} dt \right]^{\frac{1}{2k}} = \max_t \left(h_{ref} - h(t) \right) , \tag{21}$$

the minimax criterion in Eq.(21) (Chebyshev performance index) is ***approximated*** by a Bolza performance index in Ref.7 :

$$J^* = \min J = \min \int_0^{t_f} (h_{ref} - h)^n dt , \tag{22}$$

where n is a large positive, even exponent. For the best possible computational results, the reference altitude h_{ref} should be chosen as small as possible, but such that the right-hand side of Eq.(21) remains positive at all times. In Ref.7 the exponent in Eq.(22) was taken as n = 6 and the reference altitude taken as h_{ref} = 400 m.

In contrast to the above performance index ***approximation***, a transformation technique which allows to solve the ***exact*** minimax problem (20) was applied in Ref.8. More specifically, the minimax problem was converted into an equivalent optimal control problem with state variable inequality constraints and the resulting Multi-Point-Boundary-Value-Problem (MPBVP) was subsequently solved using a multiple-shooting algorithm[11].

A comparison of solutions based on the Bolza performance index approximation

("Bolza solutions") with the solutions to the original minimax problem ("Chebyshev solutions") revealed not only a marked improvement in reducing the peak value of altitude drop, but perhaps even more significantly, also the overall longitudinal behavior is radically different. In Chebyshev solutions typically altitude is traded for airspeed in the initial phase of the encounter, such as to place the aircraft in a region of relatively low downdraft.

On the other hand, the difference in lateral behavior between Chebyshev and Bolza solutions is slight only. Generally speaking it can be observed that in the final stage of a lateral escape maneuver (i.e., in the after-shear region), an aircraft ends up flying along a horizontal wind radial.

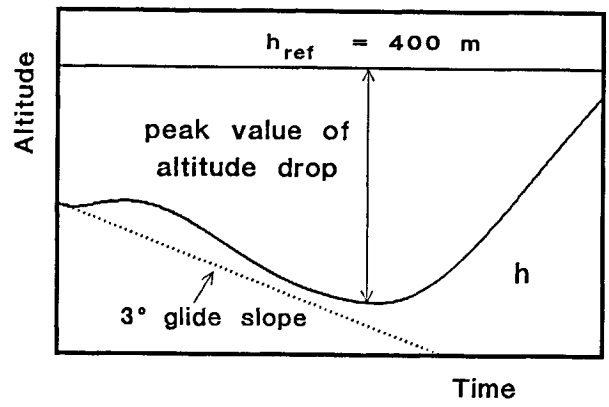

Figure 5 : Illustration of Performance Index

Based on the lessons learned from Ref.8, it is clear that, whenever possible, preference should be given to solving the minimax problem exactly. However, in view of the fact that this exact approach is mathematically rather complicated, the present study which aims at including TVFC continues to rely on the Bolza performance index approximation. However, in deviation from Ref.7, the exponent in Eq.(22) is increased from 6 to 10, in order to increase the fidelity of the solution. An analysis based on the Bolza performance index approximation, should at least give us an idea of the potential benefits of thrust vectoring vis-à-vis a fixed thrust inclination.

An appreciation for the complexity of the exact minimax approach can be obtained from the detailed study reported in Ref.12. It needs to be noted that the inclusion of thrust vectoring is likely to complicate matters even further, especially for trajectories that feature a constrained arc. Indeed, the equation for the active state-constrained arc contains the three control variables angle-of-attack, aerodynamic roll angle and the thrust-vector angle, each of which may or may not be on its limit.

In Ref.8 the performance index has been generalized in the sense that a final energy term has been included, allowing a trade-off between recovery altitude and energy. In the present study, energy management is addressed through the terminal boundary conditions.

3.2 Specification of the Boundary Conditions for the Minimax Windshear Problem

Similar to Ref.8, a single set of initial conditions has been specified in the present study. The following initial conditions (at which the escape procedure is commenced) have been assumed here :

$x(0) = x_0 = -2500$ m , $y(0) = y_0 = 0$ m ,

$h(0) = h_0 = 131$ m , $E(0) = E_0 = 384.326$ m ,

$\gamma(0) = \gamma_0 = -3°$, $\chi(0) = \chi_0 = 0°$,

$\beta(0) = \beta_0 = 0.333$

These values correspond to a situation in which an aircraft would fly during a stabilized approach (V = 70.5 m/s) without winds or windshear. It needs to be realized that in the presence of winds, the required values for γ and β will be somewhat different. The final time t_f has been set to 50 seconds, which is sufficiently long to allow a transition of the shear region.

In Ref. 8, no terminal boundary conditions on the state variables have been imposed. The main reason for that is that such conditions would mainly affect the extremal solution in the after-shear region. This can be directly attributed to the minimax nature of the problem. Indeed, once the shear-region has been passed, the setting of the controls can be chosen more or less arbitrarily, as long as the flight takes place above the previously attained minimum altitude. Although this implies that a wide range of terminal boundary conditions can be specified, this does not mean that just *any* terminal boundary can be imposed, without sacrificing recovery altitude. As a matter of fact, this has already been demonstrated in Ref.8, albeit indirectly. Indeed, Ref. 8 shows that including a relatively small end-cost term involving specific energy in the performance index, significantly influences the trajectory behavior in the after-shear region, without affecting the minimum altitude performance. On the other hand, a large specific energy end-cost term results in a huge gain in specific energy, but this comes at the expense of minimum altitude performance. Obviously, a large value of specific energy at termination can equivalently be obtained through the imposition of a terminal boundary condition. This is in fact the approach adopted herein. Whatever (terminal) energy management approach is taken, it is readily clear that the ability to gain energy is limited for a given extent (duration) of the after-shear region. Thus once the means to gain energy in the after-shear phase have been exhausted, the only way to further improve the terminal energy state is to actually limit the energy drain during the high-shear phase. Unfortunately, this boils down to trading recovery altitude for energy.

In view of the fact that thrust vectoring is not exactly beneficial in terms of specific energy conservation, we will typically specify a terminal value for specific energy in most scenario's. However, in order to get some insight into the trade-off recovery altitude versus energy, some scenario's are also recomputed without the terminal energy boundary condition.

Another aspect demonstrated in Ref.8, is that the specification of any (reasonable) terminal boundary on flight path angle has virtually no impact on the performance. This is not really surprising in view of the fact that this particular variable is capable of very

rapid transitions. Indeed, in contrast to the relatively slow process of *gaining* total energy, the process of *distributing* total energy (between kinetic energy and potential energy) brought about by transitions in the flight path angle, takes place relatively fast, and has therefore only a modest impact on the overall performance. Yet, in all scenario's considered in this study, a terminal condition for the flight path angle has been specified, primarily for "cosmetic" reasons. In summary, the following terminal boundary conditions are specified (unless stated otherwise) :

$$E(t_f) = E_f = 410 \text{ m}, \qquad \gamma(t_f) = \gamma_f = 5°$$

Note that no terminal boundary conditions for the remaining state variables have been specified. In view of the fact that a fixed flight time is considered, we do not want to a priori restrict the extremal solution too much. Obviously, the flyability of the resulting solutions is checked a posteriori.

3.3 Necessary Conditions of Optimality for the Minimax Windshear Problem

To summarize, the optimal control problem to be solved is to determine the optimal controls β^*, μ^*, α^* and δ^* such that starting from the initial conditions, the performance index of Eq.(22) is minimized for a given final time t_f, while satisfying the terminal boundary conditions and all imposed constraints.

The inclusion of δ as an additional control variable has actually only a modest impact on the necessary conditions for optimality. As a matter of fact, the original adjoint equations remain unchanged and, consequently, only the optimal control conditions need to be modified. A detailed description of the adjoint equations is presented in Ref.12 and will therefore be omitted here.

As far as the optimal control conditions are concerned, the results for aerodynamic roll angle μ and throttle setting β_t also remain unaffected. Obviously, there is a new optimal condition associated with the thrust-vector angle δ. Moreover, the optimal conditions for angle-of-attack α and thrust-vector angle δ are somewhat intertwined and therefore both conditions will be reviewed here. To this end, let us first define the Hamiltonian as :

$$\begin{aligned} H &= K(1 - \frac{h}{h_{ref}})^{10} + \lambda_x\{V\cos\gamma\cos\psi + W_x\} + \lambda_y\{V\cos\gamma\sin\psi + W_y\} \\ &+ \lambda_h\{V\sin\gamma + W_h\} + \lambda_E\{\frac{\left(T[1 - \frac{1}{2}(\alpha+\delta)^2] - D\right)V}{W} \\ &+ W_h - \frac{V}{g}[\dot{W}_x\cos\gamma\cos\psi + \dot{W}_y\cos\gamma\sin\psi + \dot{W}_h\sin\gamma]\} \\ &+ \lambda_\gamma\{\frac{g}{V}[\frac{L + T(\alpha+\delta)}{W}\cos\mu - \cos\gamma] + \frac{1}{V}[\dot{W}_x\sin\gamma\cos\psi + \dot{W}_y\sin\gamma\sin\psi - \dot{W}_h\cos\gamma]\} \\ &+ \lambda_\psi\{\frac{g}{V\cos\gamma}\frac{L + T(\alpha+\delta)}{W}\sin\mu + \frac{1}{V\cos\gamma}[\dot{W}_x\sin\psi - \dot{W}_y\cos\psi]\} + \lambda_\beta\{\frac{1}{\tau}[\beta_t - \beta]\}, \end{aligned} \tag{23}$$

where K merely represents some generic scale factor for the performance index. Assuming that both α^* and δ^* are within the interior of their admissible ranges, the following conditions apply :

$$\frac{\partial H}{\partial \alpha} = \lambda_\gamma \frac{g}{V}\frac{1}{W}[qS\frac{\partial C_L}{\partial \alpha} + T]\cos\mu + \lambda_\psi \frac{g}{V\cos\gamma}\frac{1}{W}[qS\frac{\partial C_L}{\partial \alpha} + T]\sin\mu$$
$$- \lambda_E \frac{V}{W}[T(\alpha+\delta) + qS\frac{\partial C_D}{\partial \alpha}] = 0 \quad , \tag{24}$$

$$\frac{\partial H}{\partial \delta} = \lambda_\gamma \frac{g}{V}\frac{1}{W}T\cos\mu + \lambda_\psi \frac{g}{V\cos\gamma}\frac{1}{W}T\sin\mu - \lambda_E \frac{V}{W}T(\alpha+\delta) = 0 \tag{25}$$

Substitution of Eq.(25) into Eq.(24) yields an equation in which the variable δ has been eliminated. Before carrying out this particular operation let us first use Eqs.(12) and (13) to evaluate the following terms :

$$\frac{\partial C_L}{\partial \alpha} = L_1 + 2L_2(\alpha - \alpha_{ref}) \quad , \quad \frac{\partial C_D}{\partial \alpha} = D_1 + 2D_2\alpha \tag{26}$$

Now let us define $\Phi(\mu)$ as :

$$\Phi(\mu) \triangleq \lambda_\gamma \cos\mu + (\lambda_\psi/\cos\gamma)\sin\mu \tag{27}$$

Substitution of Eqs.(26) and (27) into Eqs.(24) and (25) allows to solve for α_{uc} :

$$\alpha_{uc} = \frac{\lambda_E \frac{V^2}{g} D_1 - [L_1 - 2L_2\alpha_{ref}]\Phi}{-2\lambda_E \frac{V^2}{g} D_2 + 2L_2\Phi} \quad , \tag{28}$$

where the subscript uc is used to denote an "unconstrained" solution. It is recalled that $\Phi(\mu^*)$ can be easily obtained from the optimal control condition for aerodynamic roll angle. A comparison of Eq.(28) with the expression originally obtained for α_{uc} in the analysis involving a fixed thrust angle[12], reveals that the present expression for α_{uc} no longer directly depends on the thrust T. Substitution of Eqs.(27) and (28) into Eq.(25) yields a simple expression from which δ_{uc} can be obtained :

$$\delta_{uc} = \frac{\Phi}{\lambda_E}\frac{V^2}{g} - \alpha_{uc} \tag{29}$$

Obviously, in a severe windshear encounter both angle-of-attack and thrust-vector angle are likely to run into their respective (upper) bounds and provisions for this situation therefore have to be included in the optimal control scheme. There are several possibilities of (partial) control saturation, which all need to be considered. Let us demonstrate some of these possibilities by, for example, assuming that angle-of-attack runs into the stick-shaker limit at some point in time. Obviously, this situation occurs when the evaluation of Eq.(28) reveals that :

$$\alpha_{uc} \geq \alpha_{max} \tag{30}$$

In this case the optimal value of angle-of-attack simply is $\alpha^* = \alpha_{max}$. Note that since Eq.(24) now no longer applies, also Eq.(29) has lost its validity. However, substitution of $\alpha^* = \alpha_{max}$ into Eq.(25) now yields :

$$\delta_{pc} = \frac{\Phi}{\lambda_E}\frac{V^2}{g} - \alpha_{max} \quad , \tag{31}$$

where the subscript pc stands for "partially constrained". To find out if the thrust-vector angle computed δ_{pc} from Eq.(31) is also saturated, we must test whether $\delta_{pc} \geq \delta_{max}$. If the outcome of this test is positive, both controls will be at their respective upper limits. If the test fails, the optimal controls are : $\alpha^* = \alpha_{max}$, $\delta^* = \delta_{pc}$.

Mathematically there is one more case of interest, although from a physical perspective it is not so likely to occur. This case concerns the situation where the thrust-vector angle is already at its upper limit, while angle-of-attack has not reached the stick-shaker limit yet. In this situation we have that $\delta^* = \delta_{max}$ (Eq.(25) no longer applies), which can be substituted into Eq.(24) to get :

$$\alpha_{pc} = \frac{\lambda_E \frac{V^2}{g}[D_1 + \frac{T\delta_{max}}{qS}] - [\frac{T}{qS} + L_1 - 2L_2\alpha_{ref}]\Phi}{-2\lambda_E \frac{V^2}{g}[D_2 + \frac{T}{qS}] + 2L_2\Phi} \quad , \tag{32}$$

where obviously it must hold true that $\alpha_{pc} < \alpha_{max}$, otherwise the initial assumption of unconstrained angle-of-attack is violated. Note that Eq.(32) is exactly the same as the optimal control condition obtained in Ref.12, with the premise that the fixed thrust inclination δ now has maximum value.

In addition to control saturation at the upper limits, it is also possible that saturation at the lower control bounds occurs. Physically it is readily clear that such situations are not likely to occur within the high-shear region, but at best near the endpoints of the

trajectories. The optimal control analysis is actually easily extended to include saturation at the lower bounds, in a fashion entirely analogous to the upper bounds. However, in view of the above, this analysis will not be presented here. The lower control constraints have been fully implemented in the trajectory optimization computer program though.

In summary, four different optimal control options have been examined here :

- (Case a) unconstrained angle-of-attack and thrust-vector angle :

  $\alpha^* = \alpha_{uc}$, $\delta^* = \delta_{uc}$

- (Case b) constrained angle-of-attack and unconstrained thrust-vector angle :

  $\alpha^* = \alpha_{max}$, $\delta^* = \delta_{pc}$

- (Case c) unconstrained angle-of-attack and constrained thrust-vector angle :

  $\alpha^* = \alpha_{pc}$, $\delta^* = \delta_{max}$

- (Case d) constrained angle-of-attack and thrust-vector angle :

  $\alpha^* = \alpha_{max}$, $\delta^* = \delta_{max}$

To complete the derived Two-Point-Boundary-Value-Problem (TPBVP), the transversality conditions must be evoked to obtain the five natural (terminal) boundary conditions that supplement the nine forced boundary conditions (seven initial conditions and two terminal conditions) :

$\lambda_x(t_f) = 0$, $\lambda y(t_f) = 0$, $\lambda_h(t_f) = 0$,

$\lambda_\psi(t_f) = 0$, $\lambda_\beta(t_f) = 0$

In those scenario's where the terminal energy condition has been dropped, an additional natural boundary condition arises as :

$\lambda_E(t_f) = 0$ (only if $E(t_f)$ is free!)

In order to assess the influence on the escape procedures, different locations of the microburst have been considered in the numerical examples of Ref.6. However, since in this study the main interest is on evaluating the (relative) benefits of thrust-vectoring, the numerical examples included in this report have been limited to the single microburst location, previously selected in Ref.8. In other words, we will only consider a "symmetric" situation, with the microburst center located at (-1500 m, 0 m) on the runway centerline extension. This implies that for the given initial conditions, an aircraft in straight flight will fly exactly along the x-axis of the reference frame (see Figure 4), passing right through the microburst center.

4. Computational Results

4.1 Nonturning Scenario's

In order to investigate the characteristic features of the optimal nonturning escape trajectories, a reference scenario has been established based on the nine forced boundary conditions specified in Section 3.2 (including the terminal energy condition). In this reference scenario, thrust-vectored solutions will be compared with the solutions based on a fixed thrust inclination. Moreover, the original stake-shaker angle-of-attack limit will be assumed to apply. Next, the influences of the terminal condition on energy as well as the stick-shaker angle-of-attack limits are assessed.

We will start-off by comparing thrust-vectored and conventional AFC microburst escape trajectories for a fixed terminal energy (410 m). In Figs. 6 the results pertaining to this straight flight situation have been summarized. Since from physical considerations it is clear that full throttle should be applied during a microburst escape maneuver, the time-history of this particular control variable is not included in Figs 6. Figure 6a shows the time-history for the control variable angle-of-attack for each of the two cases. It can be seen that the angle-of-attack behavior for cases is very similar. Notably, both trajectories run into the stake-shaker limit at about the same. Figure 6b relates to the thrust-vectored solution only. It is readily seen that the thrust-vector angle starts to increase once AOA (Angle-Of-Attack) is on its limit. Moreover, the thrust-vector angle already starts to decrease well before angle-of-attack leaves its bound. As a matter of fact, the thrust-vector angle never comes near saturation. In view of the fairly limited utilization of thrust-vectoring, it is not surprising that the resulting altitude and speed profiles, shown in Figs. 6c and 6d respectively, are not markedly different either. Unfortunately, this also implies that there is virtually no improvement in recovery altitude (a disappointing 0.4 m only!). Figure 6e shows the specific energy variations during the microburst encounter. Especially in the entry phase of the encounter, the time-histories of energy are virtually indistinguishable. The minimum energy levels reached are not noticeably different either. As was to be expected, no surprises show up in the F-factor time-histories, shown in Figure 6f. Finally, Figure 6g shows that TVFC apparently dampens the path-angle variations, especially in the after-shear phase.

The results above obviously raised the question why thrust-vectoring was so scarcely applied to improve the recovery performance. It was conjectured that thrust-vectoring was simply not used because it would result in an energy bleed-off that simply can not be recovered in the final stage of the flight. This conjecture appeared to be supported by the observation that angle-of-attack leaves it limit quite early in the after-shear phase.

To find out whether this hunch was right, the above experiment was repeated, but now without the terminal energy requirement. In addition, a 1° increment in the angle-of-attack limit was also considered, such as to further explore the performance capabilities of TVFC. Some of the pertinent results related to TVFC are shown in Figure 7.

It is important to point out that four different solutions are shown in Figure 7. Two of these solutions have been generated for a fixed terminal energy level (one of which has standard AOA and one has an increased AOA limit), while in the remaining two trajectories no condition on terminal energy has been imposed. For the latter two trajectories, the distinguishing feature concerns the AOA limit only.

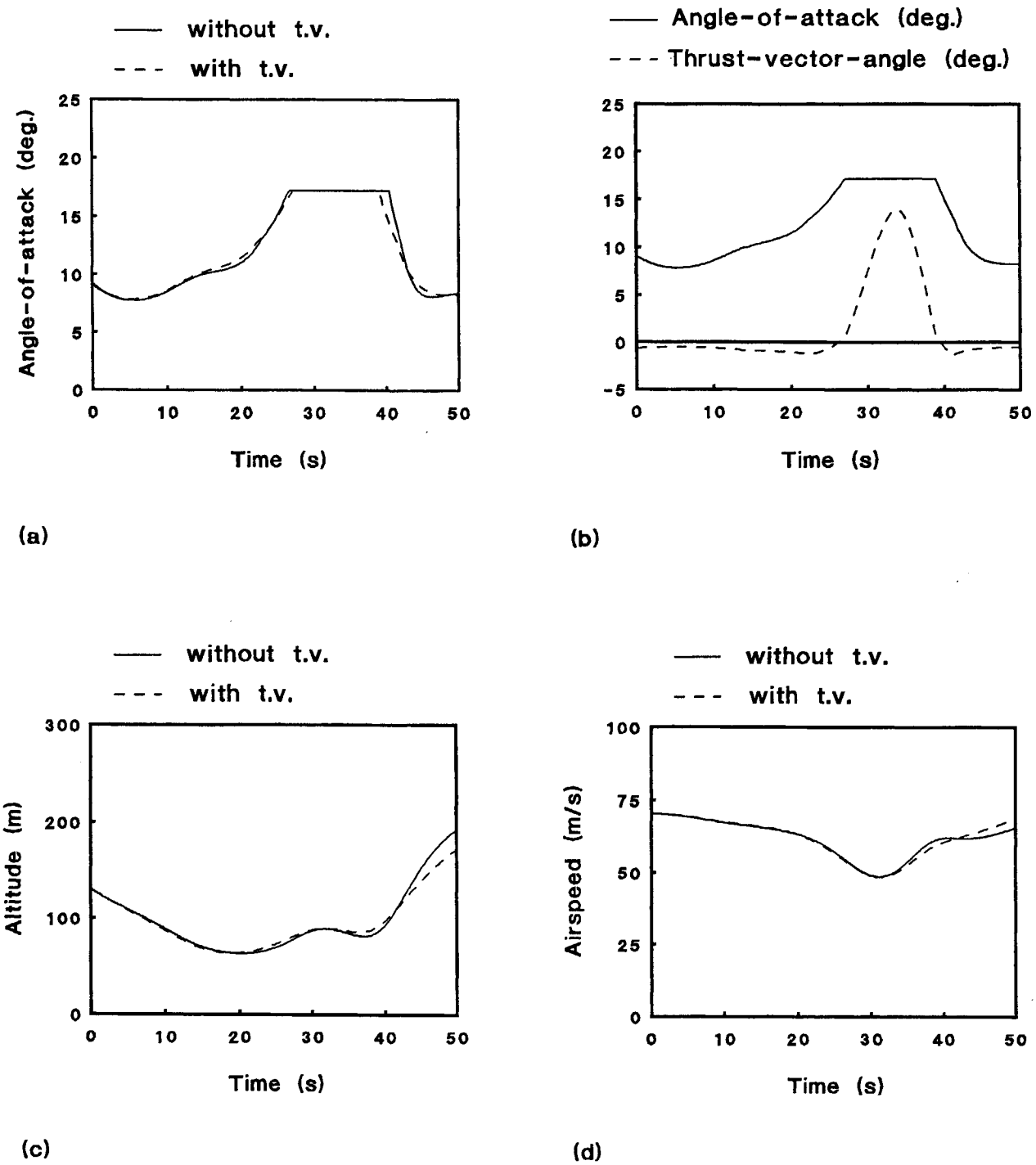

Figure 6 : Comparison of extremal solutions for a Boeing 727, with or without installed TVFC. No lateral maneuvering (μ_{max} = 0); terminal boundary condition on energy; AOA limit is 17.2°.

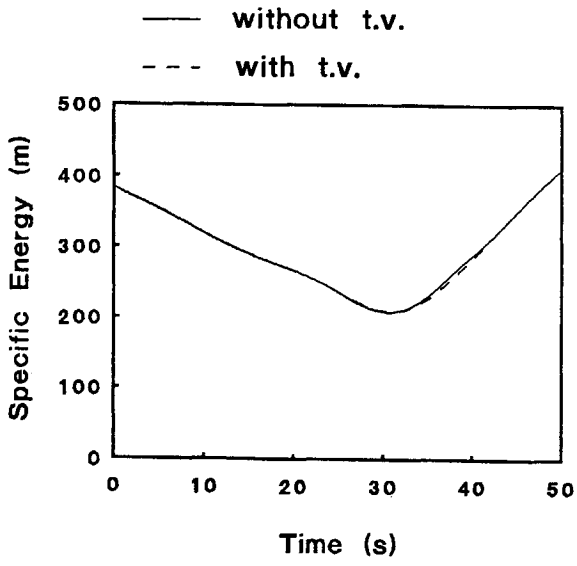

(e)

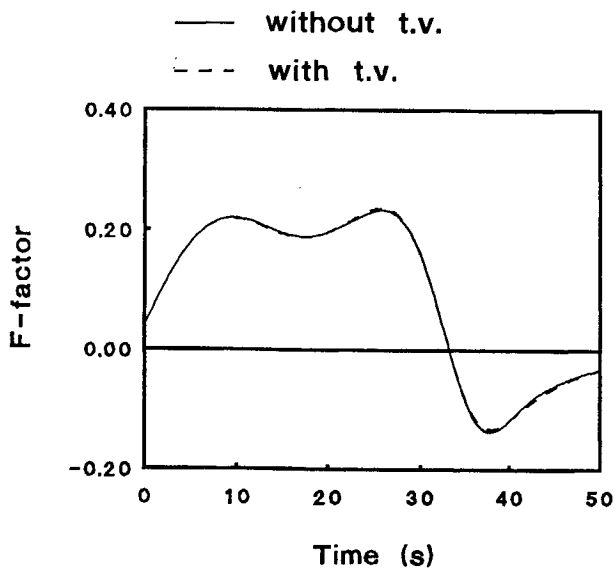

(f)

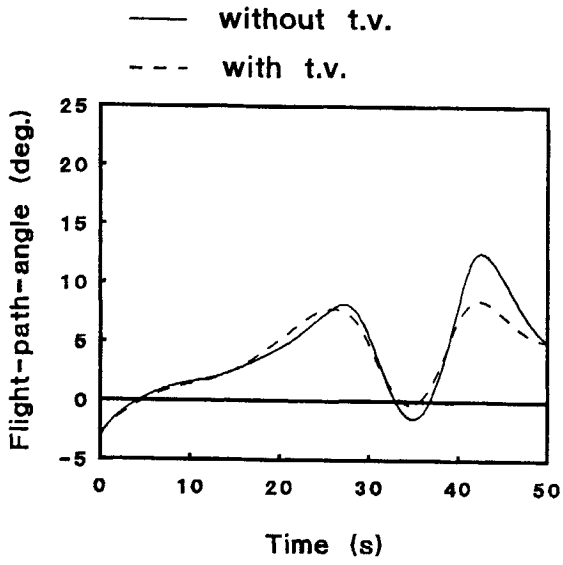

(g)

Figure 6 :
(concluded)

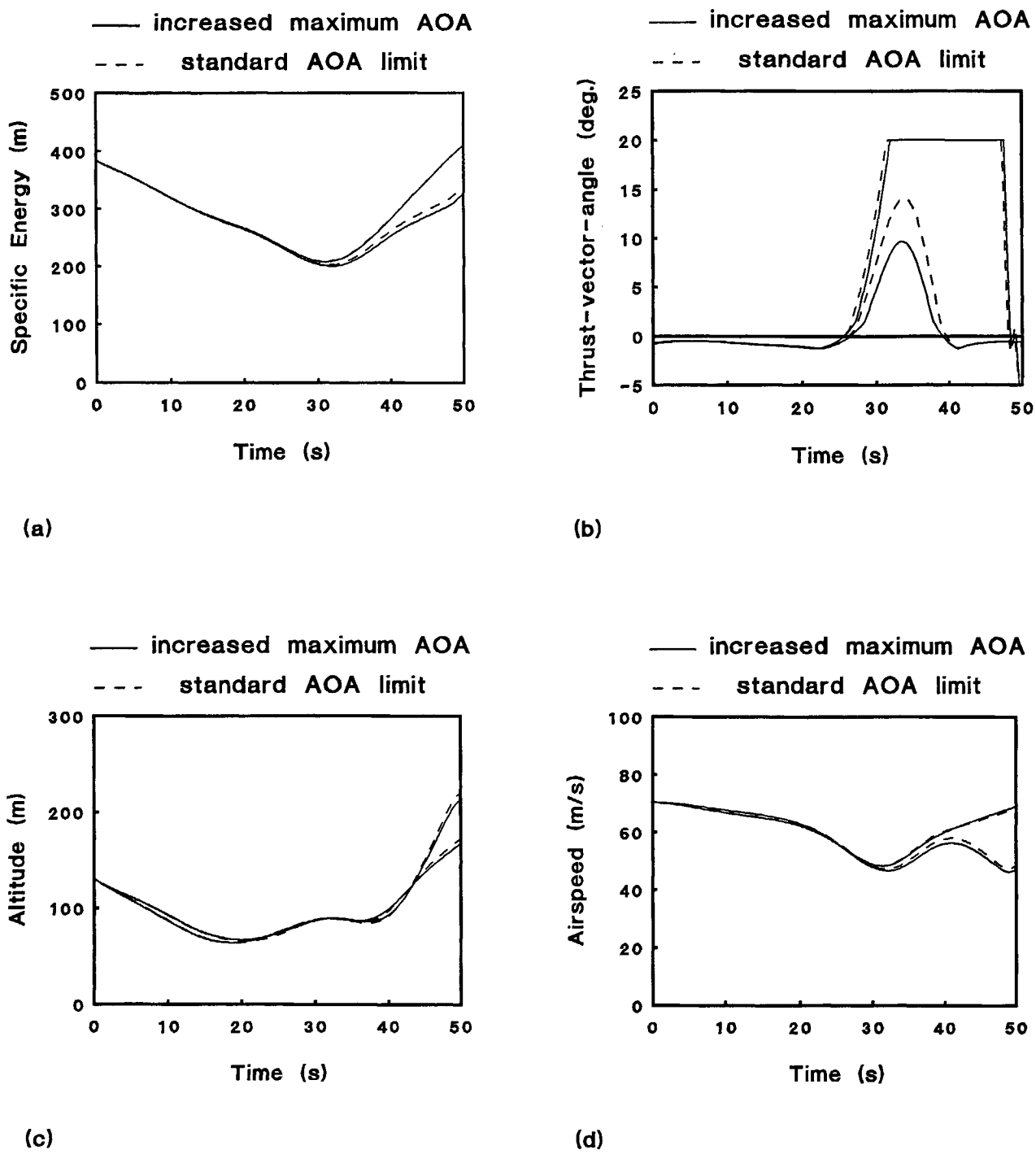

Figure 7 : Comparison of extremal solutions for a TVFC equipped Boeing 727, with and without a terminal boundary condition on energy, and with and without increased AOA limit. No lateral maneuvering ($\mu_{max} = 0$).

Figure 7a presents the four time-histories of specific energy. It is observed that the two trajectories that terminate at $E(t_f)$ = 410 m are virtually indistinguishable. Inspection of Figure 7b makes readily clear that the increment in the angle-of-attack limit has indeed even further limited TV activity. Returning to Figure 7a, it can readily be observed that the removal of the energy requirement has fairly dramatic consequences. Indeed, the energy gain in the after-shear phase is substantially lower in comparison with the fixed terminal energy trajectories. Figure 7b shows that now indeed the thrust-vector is rapidly tilted to its maximum position and remains there for quite some time. From Figure 7a it can be seen that the increased AOA limit also significantly contributes to the energy drain. Sacrificing the terminal energy does, however, have the advantage of permitting a larger energy drain within the high-shear phase, which directly translates into lower minimum speeds (see Figure 7d). The positive side of this is that the recovery altitude, our primary objective, can be modestly improved. Comparing the trajectory where both options of a free terminal energy and an increased angle-of-attack limit have been used, to the trajectory where neither option has been applied, it is found that the recovery altitude is improved by about 3.5 m (see Figure 7c). Still not a very impressive result, especially considering the price paid for it, viz., a reduction in terminal energy of 84 m. Moreover, the minimum airspeed attained at any point along the trajectory has been reduced by 1.7 m/s. Finally, unlike the fixed terminal energy solutions, the free terminal energy solutions exhibit a very undesirable behavior in the after-shear region in terms of airspeed. Worse yet, the free terminal energy solutions feature not only a low terminal speed, but also a fairly low terminal altitude.

When putting the above results into perspective, one may wonder whether the benefit (slight improvement in recovery altitude) really outweighs the cost (large reduction in terminal energy). Obviously, one can argue that avoiding low energy (low speed) situations is of less importance for TVFC equipped aircraft and to a certain extent this is indeed a valid argument. However, also for TVFC equipped aircraft there is still the need to maintain a sufficient kinetic energy reserve to avoid stall in real-life (uncertain) windshear conditions.

Figure 8 shows the time-histories of angle-of-attack corresponding to the two free terminal energy trajectories of Figure 7. Figure 7a relates to the AOA limit of 17.2°, whereas Figure 7b corresponds to an AOA limit of 18.2°. The behavior observed in the Figs. 8a and 8b is not essentially different. Thrust-vectoring only becomes prevalent once the stick-shaker limit has been reached. As a matter of fact, in all numerical examples that have been studied, we never found a situation where thrust-vector angle saturated before angle-of-attack saturated. Apparently, increasing angle-of-attack is a more efficient means to ward off the microburst than thrust-vectoring. Indeed, thrust-vectoring turns out to be no more than some sort of "last-ditch" defence.

Figure 8 also reveals a fairly peculiar behavior of the controls in the final stage of the flight. Indeed, in the final few seconds of the encounter, both the angle-of-attack and the thrust-vector angle decay rapidly. The reason for this behavior is that the terminal boundary condition on flight path angle needs to be satisfied, which calls for a low value of the angle-of-attack (dictated by the transversality conditions[12]). As a matter of fact, in the final second angle-of-attack reaches its lower bound (here arbitrarily taken as 0°). At the point where AOA runs into its lower limit, the thrust-vector angle makes a small rebound and then continues to decay, terminating at the lower bound. Evidently, the observed rapid transitions in the controls are not exactly realistic. In other words, the attempts to improve realism through the imposition of a terminal boundary condition on flight path angle have not been very successful in this free terminal energy scenario.

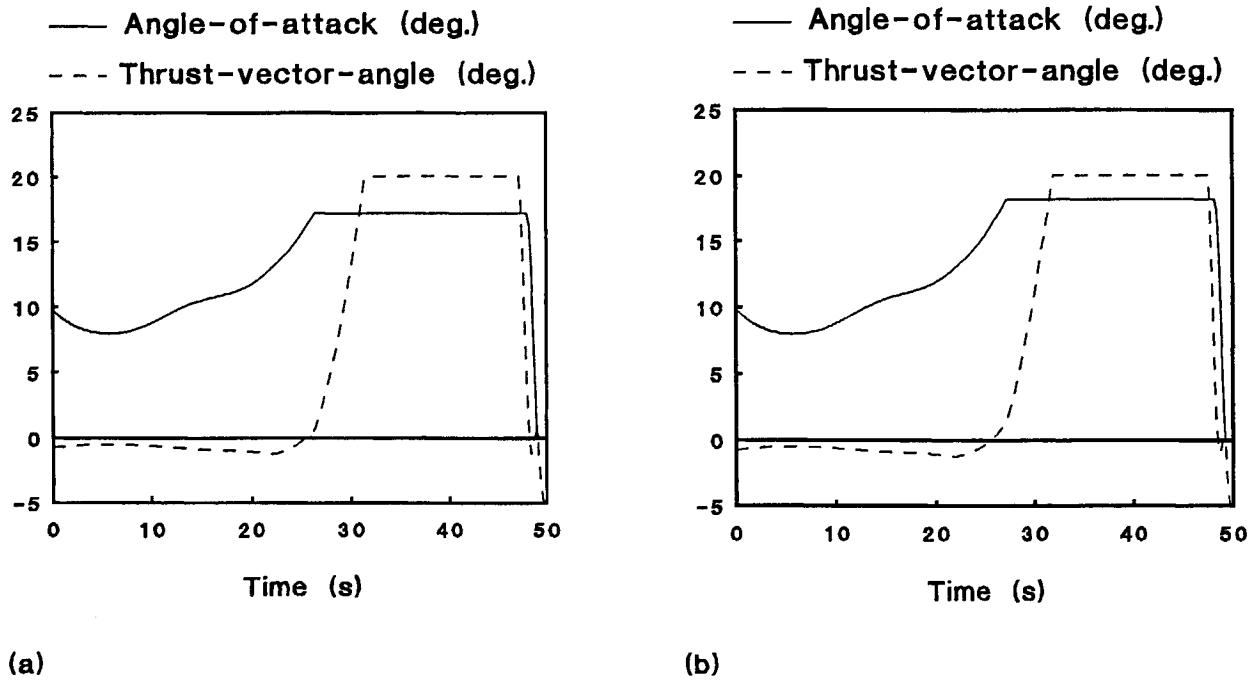

Figure 8 : Comparison of extremal solutions for a TVFC equipped Boeing 727, with and without an increased AOA limit. No lateral maneuvering (μ_{max} = 0); no terminal boundary condition on energy.

A comparison of Figure 8a and Figure 8b learns that increasing the limit on stick-shaker angle-of-attack has no discernable impact on the behavior in the high-shear region. The higher permitted value of AOA produces an improvement in recovery altitude of about 1.4 m only. The increased angle-of-attack limit also has a negative impact on the ability to gain energy in the after-shear phase, resulting in a decrease of about 13 m in the terminal value of specific energy.

4.2 Lateral Escape Scenario's

In this section, thrust-vectored escape maneuvers will be considered that feature lateral maneuvering. The usefulness of lateral escape strategies in improving the survival capability has been extensively demonstrated in previous studies[6,7,8]. The main purpose of the present lateral escape study is not so much to promote the use of lateral escape techniques, but rather to provide some sort of standard against which alternative ways to improve the microburst recovery performance can be compared.

A fairly wide range of aerodynamic roll angle limits (up to 15°) has been examined in the various lateral escape scenario's, but for reasons of conciseness only the results for the largest value in the examined range of roll angle limits will be presented. To permit a proper comparison with the straight-flight escape maneuvers presented in the previous section, the same final energy condition has been imposed, viz., $E(t_f) = 410$ m. This particular value for terminal specific energy has been selected in this study because it actually represents the *lowest* possible value attainable in a lateral escape (with a flight time of 50 seconds) that is executed with a roll angle limit of 15° and without thrust-vectoring. Obviously, it would have been possible to select a higher value for terminal energy, but this would have been less appropriate for the nonturning scenario's. Indeed, as we have seen in the previous section, it is already difficult enough to meet the imposed terminal energy requirement in straight flight.

Figure 9 shows some significant results for the lateral escape maneuver described above. As we already know from previous studies[6,7,8], higher angle-of-attack values are used in a lateral escape relative to straight flight. The relatively high initial angle-of-attack for a lateral maneuver results in a relatively high lift which, in turn, leads to a high turn rate. Clearly, a high initial turn rate is desired to direct the aircraft away from the microburst center. On the other hand, it is also desirable to keep the energy bleed-off (and thus drag) as modest as possible. The optimization process attempts to establish the overall best compromise between those two conflicting requirements. Comparing Figure 9a with the nonturning counterpart in Figure 6a, it is clear that the lateral escape maneuvers feature a much longer stay at the stick-shaker limit. In a lateral escape, the observed difference in angle-of-attack behavior between thrust-vectored and conventional flight is very small, with the largest differences occurring well in the after-shear region. However, Figure 9b makes clear that, in contrast to straight flight (see Figure 6b), the thrust-vector is significantly deflected when called upon. This shows that indeed the terminal energy requirement is not a truly demanding factor in this lateral escape maneuver.

Figure 9c shows that the more extensive use of thrust-vectoring does result in a slight improvement in recovery altitude. While in straight flight the improvement in recovery altitude due to TVFC was only 0.4 m, in the lateral escape an improvement of some 4 m resulted. A more detailed analysis has shown that the improvement brought about by thrust-vectoring indeed increases with the permitted aerodynamic roll angle limit. The results are summarized in Figure 10. A closer inspection learns that the recovery altitude improvements can be directly attributed to the increased TVFC activity in lateral escape maneuvers. In turn, this increased TVFC is possible due to the fact that in a lateral escape maneuver, more time is available to recover from the energy dissipation caused by windshear exposure. A comparison of the time-histories of energy for nonturning (Figure 6e) and turning (Figure 9e) maneuvers reveals that the point of minimum energy is reached some 4 seconds earlier in a lateral escape. Moreover, the minimum energy level is somewhat higher in a lateral escape, especially when TVFC is not used.

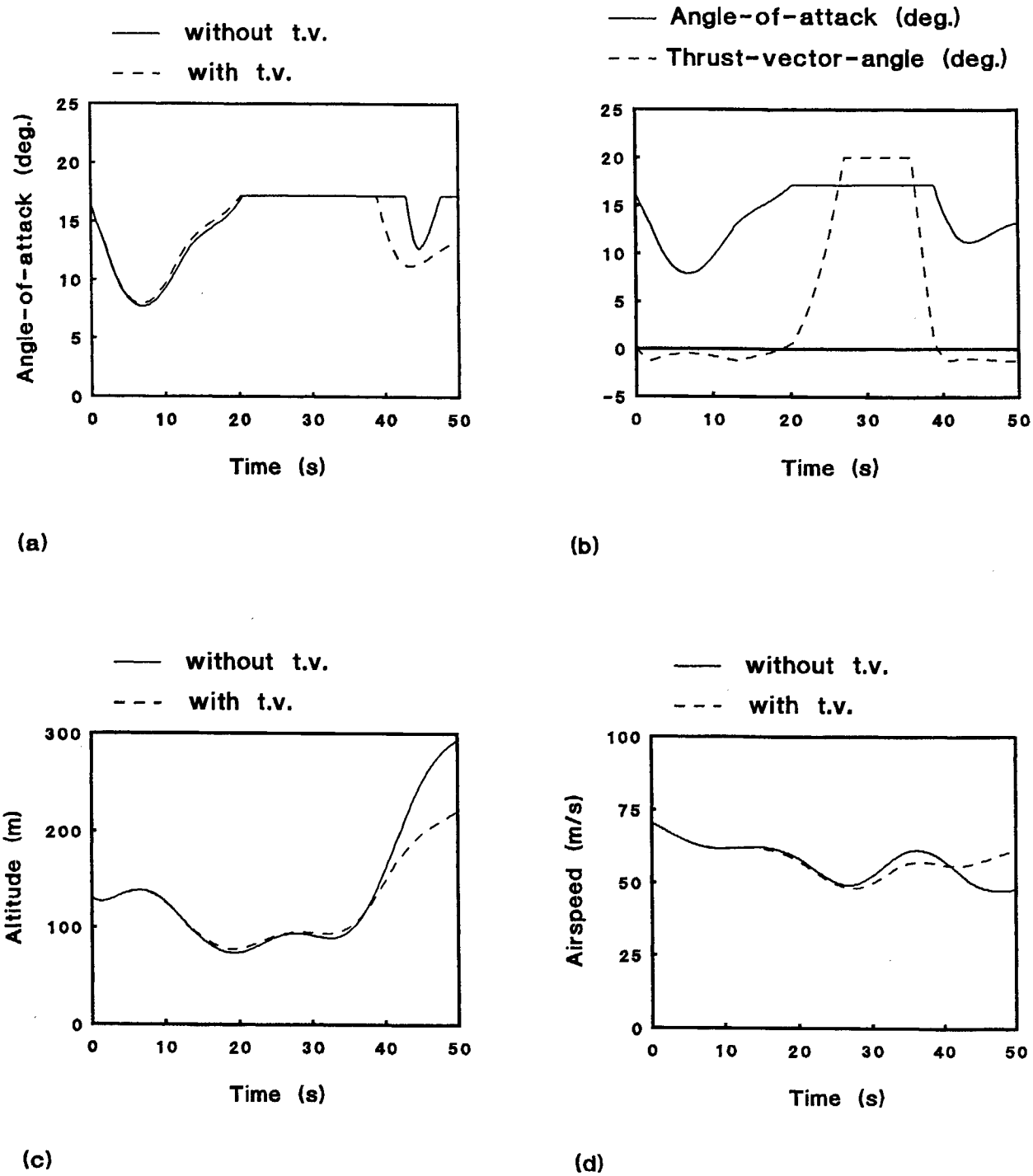

Figure 9 : Comparison of extremal solutions for a Boeing 727, with or without installed TVFC. Lateral maneuvering (μ_{max} = 15°); terminal boundary condition on energy; AOA limit is 17.2°.

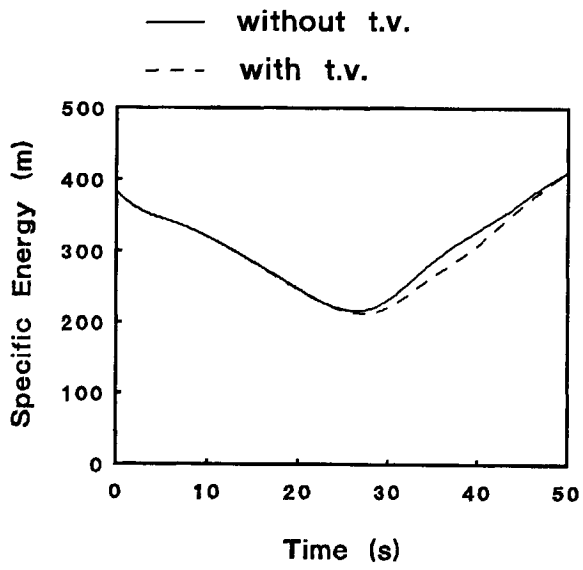

(e)

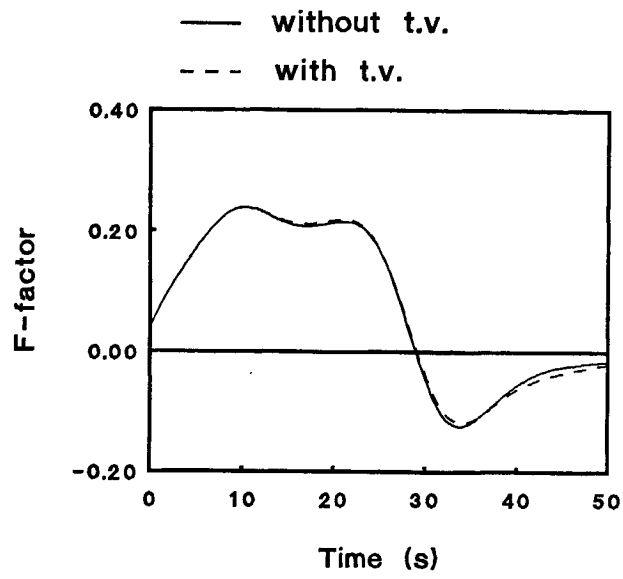

(f)

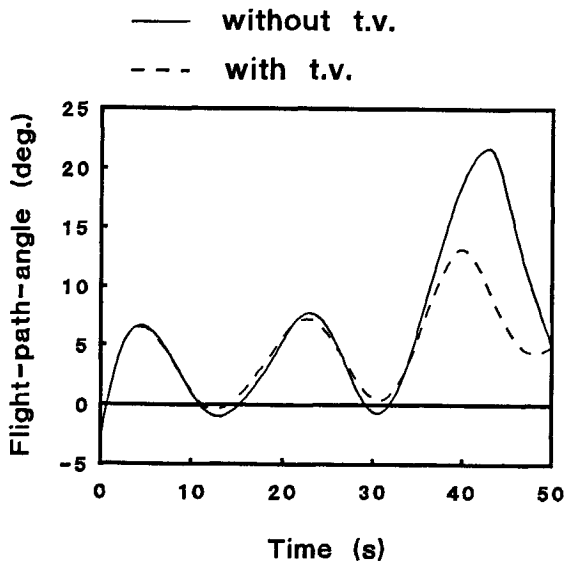

(g)

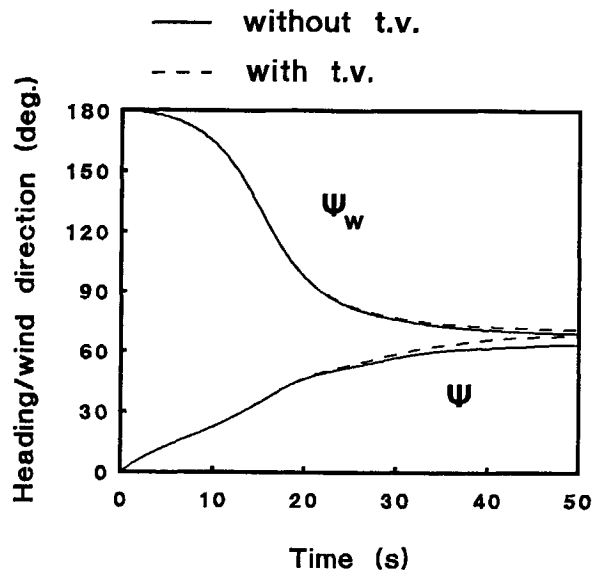

(h)

Figure 9 :
(continued)

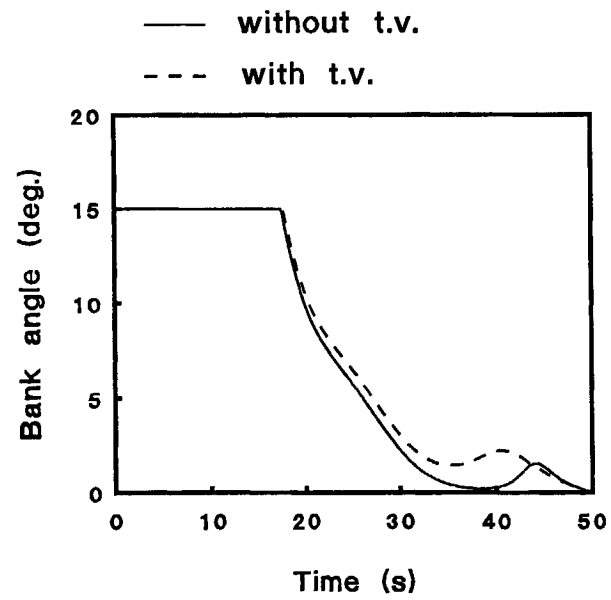

(i)

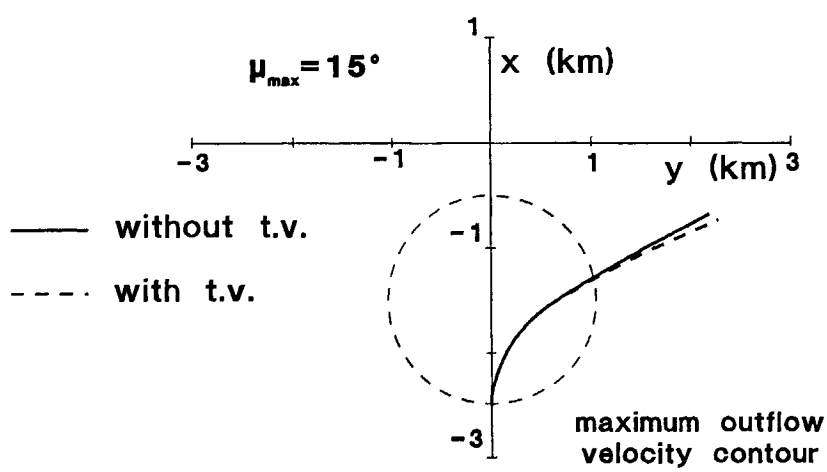

(j)

Figure 9 :
(concluded)

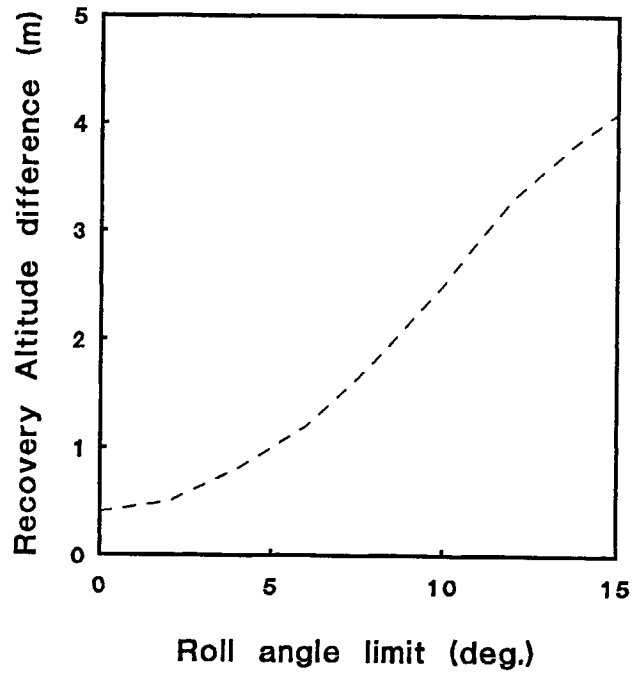

Figure 10 : Improvement in recovery altitude as a function of the aerodynamic roll angle limit for a Boeing 727 with installed TVFC. Terminal boundary condition on energy; AOA limit is 17.2°.

Although the recovery altitude improvement brought about by TVFC is some 4 m, this gain is still small in comparison with the gain that can be obtained by switching from a straight-ahead escape to a lateral escape. To see this more clearly, compare e.g. the results in Figure 9c with those in Figure 6c. The results show that for the Boeing 727 (without TVFC) the improvement in recovery altitude is of the order of 10 m. Obviously, the performance benefit of the lateral escape can become even more pronounced if larger values of the aerodynamic roll angle are permitted.

Figure 9d depicts the time-history of airspeed. It is seen that the application of TVFC results in a slightly lower airspeed (a difference of about 1.5 m/s) in the high-shear region. However, in the trajectory where no TVFC has been used, the lowest speed does not occur in the high-shear region but in the after-shear region. As a matter of fact, the minimum airspeed observed in the conventional escape maneuver is even lower than in the TVFC-aided escape. These low speeds in the after-shear region are the result of a phugoid motion, induced by flying at or near the angle-of-attack stick-shaker limit. This phugoid behavior is perhaps best illustrated in the time-history of flight path angle shown in Figure 9g. In Figure 9g it is also seen that the application of TVFC dramatically curtails the flight path angle excursion.

One of the more interesting observations that can be made relates to the fact that in a lateral escape TVFC apparently allows a better energy recovery in the after-shear phase (see Figure 9e). Figure 9f shows that this can probably be attributed to better F-factor levels in the final 10 seconds of the flight. In turn, the slightly lower F-factor values in the final stage (recall that a negative F-factor value corresponds to an energy gain!) are a direct result of the fact that in TVFC-aided escape maneuver the "heading error" is closed much faster. Note that heading error is defined as the relative horizontal wind direction (i.e., the difference between the radial wind direction and the actual heading). From previous studies[6,7,8], we know that when an aircraft is flying in the after-shear region (outside the peak radial outflow-velocity contour), the best performance is achieved by flying along a "wind radial". Figure 9i shows that the improved wind radial alignment is caused by slightly increasing the roll angle in the final phase. The observed roll behavior seems to be somewhat peculiar, but it has to be realized that once altitude has been sufficiently recovered, the emphasis in the optimization process can be shifted towards meeting the terminal energy requirement. Finally, in Figure 9j the ground tracks of the lateral escape maneuvers are shown. The tracks readily reveal the short-cut within the high-shear region, explaining the more favorable energy management obtained through lateral maneuvering. Note also here that the influence of TVFC is visible outside the peak outflow contour only.

It has to be noted that originally some more scenario's have been contemplated, including some that are representative of forward-look detection cases. However, since it was felt that the impact of TVFC can be sufficiently understood from the examples considered thus far, the additional scenario's will no longer be pursued.

5. Conclusions and Recommendations for Future Research

In this report a preliminary study on the usefulness of the application of thrust-vectoring for microburst escape maneuvers for civil aircraft has been presented. A realistic model describing the point-mass dynamics of a Boeing 727 type aircraft was used for this purpose. TVFC was introduced in the form of a thrust deflection angle that could be varied from -5° to +25°. The considered aircraft type is particularly suited for TVFC, since it features rear-mounted engines that offer a fairly large pitch-moment arm, so that vectored thrust can provide the angular accelerations so desperately needed in critical (low speed) situations where aerodynamic controls are no longer effective. Thrust vectoring can thus be a very useful capability to recover from a stall condition, which may possibly result from a severe microburst encounter at low altitude.

However, stall recovery has not been the focus of our study. In contrast, stall prevention by respecting the stake-shaker angle-of-attack limit at all times has been the fundamental assumption upon which this optimization study has been based. This implies that not so much the capability of TVFC to generate pitch-moments has been of interest, but rather the capability to augment the aerodynamic lift in critical low-speed situations that result when a severe microburst is penetrated. The idea here was that by augmenting the lift with a thrust component, the altitude loss in a microburst encounter could be improved. A priori it was realized that any recovery altitude improvement would be modest, due to the limited magnitude of the thrust-vector component in lift direction that can be provided by a commercial aircraft such as the Boeing 727. Moreover, the use of TVFC to augment lift is inherently accompanied with a reduction in the capability to improve the energy state of the aircraft. An energy buffer in the form of an airspeed reserve is important, since it makes an aircraft less vulnerable to uncertainties in microburst intensity and extent. The main purpose of the present study therefore essentially boils down to performing a performance trade-off between recovery altitude and energy preservation.

The numerical experiments revealed that thrust vectoring can indeed produce a slight improvement in recovery altitude, provided that no (significant) attention is paid to energy preservation. The improvements in recovery altitude that can be brought about are of the order of 3 to 4 m, for the scenario's considered. Lateral escape maneuvers benefit only slightly more from TVFC. However, lateral maneuvers are vastly superior in terms of recovery altitude as well as energy preservation. Indeed, the results show that by switching from a straight-ahead escape to a lateral escape the improvement in recovery altitude easily exceeds 10 m, while improving the energy behavior. It can thus be concluded that as far as safety improvement is concerned, lateral maneuvering is far more effective than TVFC.

Energy preservation indeed turns out to be a concern when TVFC is employed. To deal with the problem of energy loss, a boundary condition on terminal energy has been introduced. Unfortunately, the specification of such an energy constraint may take its toll on TVFC deployment. Indeed, when a terminal value of energy is specified that is significantly above the terminal energy level found in a free terminal energy solution, TVFC activity is significantly reduced to limit the energy bleed-off. Obviously, this implies that the positive effect of TVFC on recovery altitude vanishes as well. In the present study this particular behavior can be readily observed in the straight-ahead escape. On the other hand, in the lateral escape scenario the specified terminal energy is sufficient close to the free terminal energy value so that TVFC can still be fully utilized. It is clear that when the specified terminal value of specific energy would be further increased, that

eventually also in a lateral escape the TVFC activity, and thus the associated benefits, would gradually diminish as well.

One of the main benefits of the use of TVFC is that it would allow the use of higher values of angle-of-attack. Our findings indicate that the recovery altitude can indeed be modestly improved, but, unfortunately, this comes at the expense of a relatively large terminal energy loss. It is conjectured here that this unexpectedly disappointing behavior may be related to the fact the relationship lift-coefficient vs. angle-of-attack is nonlinear in the high angle-of-attack region. As a consequence, the lift-to-drag suffers when the stick-shaker angle-of-attack limit is increased.

It has to be noted that the minimax study presented herein is not entirely exact in the sense that the original minimax criterion has been approximated by a Bolza performance index. The idea here was that, before undertaking the more elaborate exact minimax analysis, it would be useful to first identify potential advantages using the Bolza performance index approximation, for which the optimal solution is far easier to obtain. However, the results established in this study do not hold out great promise for TVFC as a useful means to truly improve windshear recovery and, as a result, we do not consider it worth while to undertake the exact minimax analysis at this stage. The decisive factor that has ultimately led to this conclusion is that, unlike lateral maneuvering, TVFC dramatically compromises the ability to manage specific energy during recovery.

References

1. Gal-Or, B., "Civilizing Military Thrust Vectoring Flight Control", *Aerospace America*, April 1996, pp.20-21.
2. Gal-Or, B., "Thrust Vector Control Eyed for Passenger Aircraft: A Novel Methodology to Combine Jet-Engine Tests with Sub-Scale Proof-of-Concept Flight Tests", *International Journal of Turbo and Jet Engines*, Vol.11, No. 1/2, 1994, pp. 1-9.
3. Veen, E.M., van der, "Civil Applications of Thrust Vectoring - An Exploration", paper to be presented at 21th ICAS Congress, Melbourne, Australia, 1998.
4. *Windshear Training Aid*, U.S. Department of Transportation, Federal Aviation Administration, Washington D.C., 1987.
5. Miele, A., Wang, T., Melvin, W.W. and Bowles, R.L., "Acceleration, Gamma and Theta Guidance for Abort Landing in a Windshear," *Journal of Guidance, Control, and Dynamics*, Vol.12, Nov.-Dec. 1989, pp. 815-821.
6. H.G. Visser, "Lateral Escape Guidance Strategies for Microburst Windshear Encounters", *Journal of Aircraft*, Vol. 33, July-August 1997, pp. 514-521..
7. H.G. Visser, "Optimal Lateral Escape Maneuvers for Microburst Encounters During Final Approach," *J. Guidance, Control and Dynamics*, Vol. 17, Nov.-Dec. 1994, pp. 1234-1240.
8. H.G. Visser, "A Minimax Optimal Control Analysis of Lateral Escape Maneuvers for Microburst Encounters", *J. Guidance, Control and Dynamics*, Vol. 20, March-April 1997, pp. 370-376.
9. Miele, A., Wang, T. and Melvin, W.W., "Optimization and Acceleration Guidance of Flight Trajectories in a Windshear," *Journal of Guidance, Control, and Dynamics*, Vol.10, July-August 1987, pp. 368-377.
10. Miele, A., Wang, T. and Melvin, W.W., "Penetration Landing Guidance Trajectories in the Presence of Windshear," *Journal of Guidance, Control, and Dynamics*, Vol.12, Nov.-Dec. 1989, pp. 806-814.
11. Grimm, W., Berger, E. and Oberle, H.J., "Benutzeranleitung fur das Rechenprogram BNDSCO zur Lösung Beschrankter Optimaler Steuerungsprobleme", DFVLR-Mitt. 85-05, 1984.
12. Visser, H.G., "A Minimax Optimal Control Analysis of Lateral Escape Maneuvers for Microburst Encounters," Memorandum M–713, Delft University of Technology, Nov. 1995.

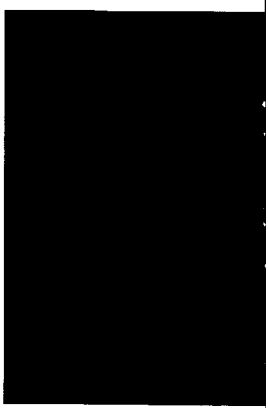

Memorandum 845

60142021210